Process Safety and Environmental Protection 193 (2025) 272–285

Contents lists available at ScienceDirect

Process Safety and Environmental Protection

journal homepage: www.journals.elsevier.com/process-safety-and-environmental-protection

Degradation of hemihydrate phosphogypsum-based backfill in underground mining: Mechanical and microstructural insights on the effects of pH and temperature of mine water

Zhikai Wang [a,b], Yiming Wang [a,*], Giovanna Antonella Dino [b], Lianfu Zhang [c,*], Zhuen Ruan [a], Minzhe Zhang [a], Jianqiu Li [d], Aixiang Wu [a]

[a] School of Civil and Resources Engineering, University of Science and Technology Beijing, Beijing 100083, China
[b] Department of Earth Sciences, University of Torino, Torino 10125, Italy
[c] School of Mining Engineering, Anhui University of Science and Technology, Huainan 232001, China
[d] Guizhou Chanhen Chemical Corporation, Fuquan 550500, China

ARTICLE INFO

Keywords:
Mine backfill
Phosphogypsum disposal
Temperature effects
PH effects
Mechanical strength
Microstructure

ABSTRACT

The mechanical properties of hemihydrate phosphogypsum-based backfill (HPG-backfill) are significantly influenced by the temperature and pH of mine water (MW), impacting the stability of underground mining operations. This study evaluates the effects of MW at different temperatures (20°C, 30°C, and 40°C) and pH levels (3, 5, and 7) on HPG-backfill's mechanical strength. A comprehensive analysis, including uniaxial compressive strength (UCS) testing, scanning electron microscopy (SEM), X-ray diffraction (XRD), thermogravimetric and differential thermogravimetric (TG-DTG), and nuclear magnetic resonance (NMR), was employed to explore degradation mechanisms. The results indicate a significant decline in the mechanical performance of HPG-backfill when exposed to MW. This degradation becomes particularly pronounced under more acidic conditions and at elevated temperatures. A polynomial relationship between strength and pH, and a linear correlation with temperature, were identified. Interaction effects between temperature and pH on 28-day strength degradation were observed, diminishing with increased temperature or decreased pH. Gray relational analysis highlights pH as a more critical factor than temperature in degradation. Strength degradation is primarily attributed to gypsum dissolution and the pressure induced by recrystallization, which leads to the formation of fatigue cracks. Additionally, acidic conditions accelerate premature crystallization, altering both the crystal morphology and the pore structure. These insights advance the understanding of HPG-backfill degradation, guiding the developing of more resilient backfill materials for extreme mining environments.

1. Introduction

The effective disposal and utilization of phosphogypsum (PG), a major byproduct of the phosphate chemical industry, remains a pressing environmental challenge (Jia et al., 2021; Zhang et al., 2021a,b; Zhou et al., 2020). Traditionally, PG disposal involves simple washing and filtration, followed by surface stacking, which results in wasted land and environmental contamination from residual acids, saline water, harmful ions, and organic pollutants (Bouargane et al., 2023; Wang et al., 2023a, c). Although many researchers have explored the comprehensive utilization of PG for producing soil amendments, cement retarders, and road base materials (Degirmenci et al., 2007; Kacimi et al., 2006; Meskini et al., 2021; Zhao et al., 2021), its utilization rate remains low at only 15 % (El-Didamony et al., 2013; Holanda et al., 2017). Consequently, countries worldwide, including China, are seeking environmentally friendly, large-scale method for PG disposal. One promising approach is using PG as backfill aggregate for underground filling (Li et al., 2017). However, conventional PG backfilling primarily uses cement as a binder (Shi et al., 2021), which is not economically sustainable for mining companies. Jiang et al. (2018a) enhanced the wet-process phosphoric acid production process by increasing the reaction temperature and phosphoric acid concentration, converting PG from the dihydrate to the

* Correspondence to: School of Civil and Environmental Engineering, University of Science and Technology Beijing, Beijing 100083, China.
E-mail addresses: zhikai.wang@unito.it (Z. Wang), ustbwym@126.com (Y. Wang), giovanna.dino@unito.it (G.A. Dino), lfzhang@aust.edu.cn (L. Zhang), ustb_ruanzhuen@ustb.edu.cn (Z. Ruan), 383198946@qq.com (M. Zhang), lijc@chanhen.com (J. Li), wuaixiang@126.com (A. Wu).

https://doi.org/10.1016/j.psep.2024.11.003
Received 22 September 2024; Received in revised form 31 October 2024; Accepted 1 November 2024
Available online 8 November 2024

hemihydrate form. The resulting industrial waste, hemihydrate phosphogypsum (HPG), consists primarily of hemihydrate gypsum with certain cementitious properties, making it a viable substitute for cement in underground backfilling. This method effectively addresses high disposal costs and low utilization rates of PG.

The mechanical properties of backfill, which are crucial to its stability, are influenced by various factors, such as the binder-to-aggregate ratio, mass concentration, curing time, and porosity (Jiang et al., 2024; Kasap et al., 2023; Naik et al., 2006; Sari et al., 2023; Wang et al., 2023b, 2024c). In addition to these internal factors, the external environment, particularly the pH and temperature of mine water (MW), significantly affects backfill performance (Wang et al., 2020; Wang et al., 2020; Zhang et al., 2021a,b). Fig. 1 illustrates the formation of MW at mining sites. MW can vary widely, from clean to highly mineralized, and may contain pollutants or exhibit acidic properties (Yu et al., 2015; Zhao et al., 2020). Acidic MW has been shown to degrade the microstructure and mechanical integrity of backfill materials, threatening the stability of underground operations (Arjomandi et al., 2023; Davila et al., 2021; Shariati et al., 2023). As mining operations extend to greater depths, higher geothermal gradients lead to elevated water temperatures, which can exacerbate the effects of acidic conditions on backfill stability (Khanal et al., 2022). Studies indicate that rock temperatures may reach 30–45°C, or even higher, in deep mining operations, as shown in Fig. 2, where MW can also exhibit highly acidic characteristics (Deng and Xiao, 2024; He and Guo, 2013; Zhang et al., 2024).

Understanding how pH and temperature affect HPG-backfill is crucial for ensuring the safe and effective use of backfill materials in modern mining. Recent studies have shown that cementitious materials are highly susceptible to degradation under acidic and elevated temperature conditions (Ren et al., 2022; Tran et al., 2021; Visrudi and Sharifi, 2023). These studies highlight the accelerated leaching of calcium and the dissolution of key hydration products under acidic conditions, as well as the increased rate of chemical reactions at higher temperatures (Aiken et al., 2018; Fall et al., 2010; Qu et al., 2021). However, the specific behavior of HPG-backfill under these conditions remains underexplored, particularly concerning the combined influence of pH and temperature on its microstructural integrity.

Temperature and pH are fundamental environmental parameters that can accelerate chemical reactions, affect material degradation, ultimately affecting the stability of backfill structures. While MW typically contains dissolved ions that may also impact backfill performance, this study narrows its focus to the effects of pH and temperature, two of the most critical factors in the environmental degradation of materials (Chen et al., 2017; Zhang et al., 2021a,b). This research systematically investigates the effects of pH and temperature on HPG-backfill, focusing on these variables to minimize confounding factors.

Given the above, this study investigates the effects of MW temperature (20°C, 30°C, and 40°C) and pH (3, 5, and 7) on the mechanical strength and degradation mechanisms of HPG-backfill. It focuses on the immediate impact of these common environmental factors in mining operations. The originality of this research lies in its comprehensive examination of how temperature and pH influence HPG-backfill stability, an area insufficiently explored in previous studies. By simulating real-world MW conditions in a controlled setting, the study evaluates changes in strength, mass loss, appearance, and microstructural integrity to reveal potential degradation mechanisms. The core objective is to clarify how different MW conditions affect the mechanical properties of HPG-backfill, providing practical guidelines for its application in mining environments. These findings also support future research into additional factors, such as MW ionic composition, to further understand how these variables impact HPG-backfill stability.

2. Materials and methods

2.1. Raw materials

The materials used in this study, including HPG, tailings, and quicklime, were provided by Chanhen Chemical Co., Ltd. in Guizhou, China.

The chemical compositions of these materials were determined using X-ray fluorescence, with the results presented in Fig. 3. HPG mainly consists of CaO, SO_3, and SiO_2, while tailings are predominantly composed of SiO_2. Quicklime, which serves as an alkaline modifier, has an effective CaO content of 72.6 % (Jiang et al., 2022b). The particle size distributions of these materials were measured using a particle size analyzer (Mastersizer 2000, Malvern, UK), with the results shown in Fig. 4. Local tap water was used as mixing water.

2.2. Sample and MW preparation

This study is limited to small-scale laboratory samples, focusing solely on the pH and temperature factors of MW, without considering the complex interactions that occur in large-scale underground mining environments.

To simulate the effects of MW at different pH levels and temperatures, deionized water was used as the base, and industrial sulfuric acid was added to adjust the pH, following the guidelines in Chinese standard GB/T 534–2014. This approach eliminated the influence of other ions typically present in MW, as mentioned in the introduction. The pH of MW typically ranges from 3.26 to 8.18 (Bharat et al., 2024), so MW was prepared at pH levels of 3, 5, and 7 to reflect realistic mining conditions. A pH of 3 simulates acid MW, commonly found in sulfide mineral mines,

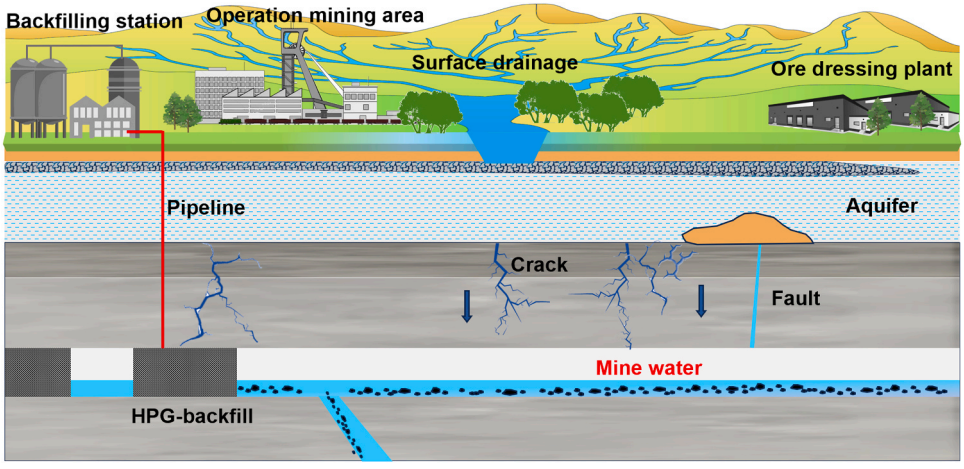

Fig. 1. Schematic diagram illustrating the formation of MW in mining sites.

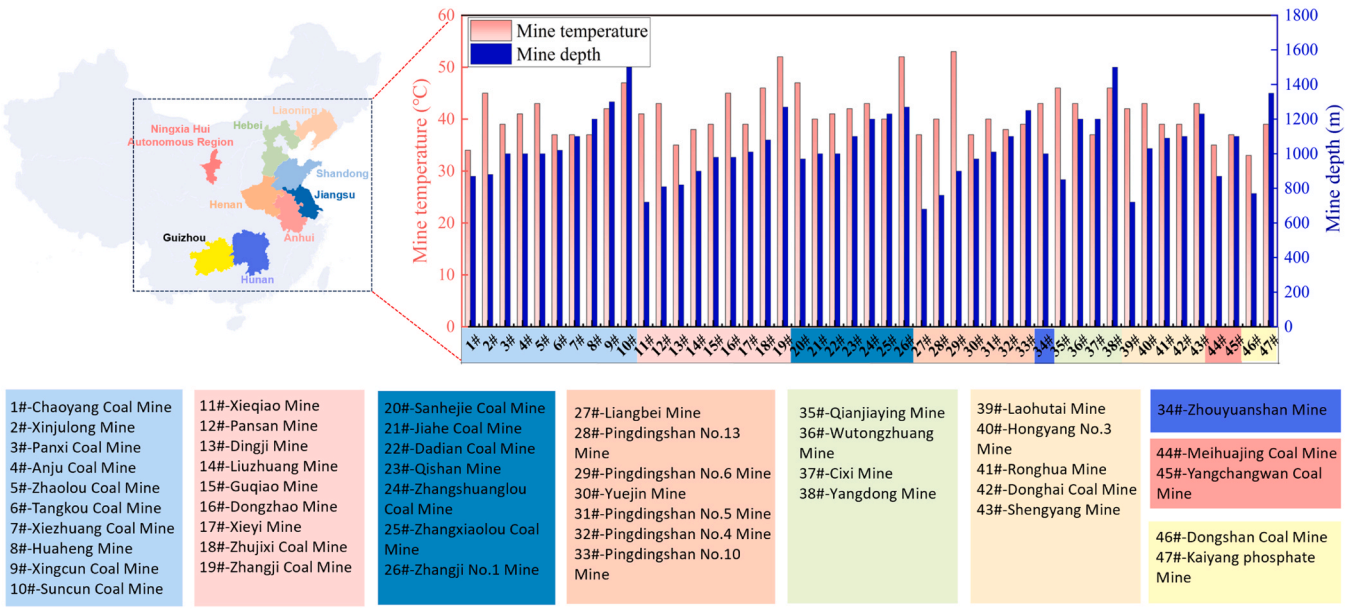

Fig. 2. The situation of mine depth and MW temperature in some provinces of China.

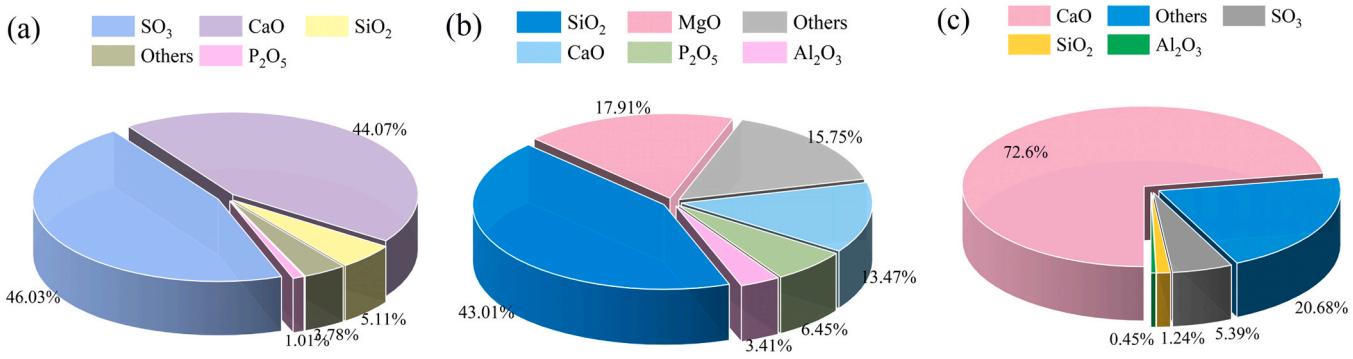

Fig. 3. Chemical composition of raw materials: (a) HPG; (b) Tailings; (c) Quicklime.

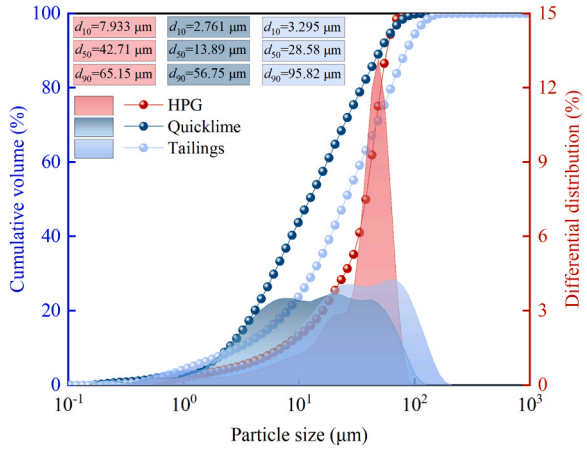

Fig. 4. The particle size distribution of tested materials.

where highly acidic conditions lead to significant material degradation. A pH of 5 represents mildly acidic conditions that can result from natural processes, such as silicate weathering, or from anthropogenic sources like pollutants. Meanwhile, a pH of 7 reflects neutral conditions, often buffered by surrounding geological materials.

Similarly, temperatures of 20°C, 30°C, and 40°C were chosen to represent ambient, elevated, and extreme underground mining conditions, which may arise due to active mining operations or chemical reactions, as shown in Fig. 2. The liquid-solid ratio of 2:1 was carefully chosen to ensure effective interaction between the MW and the HPG-backfill material. This ratio allows sufficient MW to permeate the backfill, enabling a thorough evaluation of the effects of different pH levels and temperatures on its mechanical strength and microstructural integrity. The pH was monitored and adjusted every four days using additional sulfuric acid to maintain consistency. Temperature control was achieved using a water bath for 30±2 C and 40±2°C conditions, and an air-conditioned room was used for 20°C, ensuring a stable environment throughout the experiment.

To evaluate the effects of MW pH and temperature on the mechanical properties of HPG-backfill, samples were prepared according to specified material proportions. In each experimental group, the mass concentration of HPG-backfill was maintained at 66 %, which included 4 % quicklime and 10 % tailings based on the mass of HPG. The material composition consisted of 1000 g of HPG, 40 g of quicklime, 100 g of tailings, and 587 g of tap water. These materials were mixed thoroughly for 5 min in a cement mortar mixer to form a uniform slurry. The slurry was then poured into triple test molds with dimensions of 70.7 mm × 70.7 mm × 70.7 mm. For each test group, three parallel samples were prepared to ensure reliability and reproducibility, reducing potential experimental error related to pH and temperature effects. Results were

analyzed based on the averaged values of these parallel samples.

The experimental design is presented in Table 1. N1 serves as the control group with no exposure to MW. Experimental groups N2 to N10 are exposed to different MW conditions, specifically with differences in pH and temperature. In groups N2 to N4, the pH remains neutral (pH=7), while the temperature progressively increases from 20°C to 40°C. Groups N5 to N7 are exposed to a more acidic environment (pH=5), with temperatures also ranging from 20°C to 40°C. Lastly, groups N8 to N10 are subjected to the most acidic conditions (pH=3), with temperatures again increasing from 20°C to 40°C. These variations facilitate the evaluation of the effects of different MW conditions on the mechanical properties of the backfill, specifically in relation to pH and temperature changes.

2.3. Test methods

The study employed various methods to assess the effects of MW at different temperatures and pH levels on the mechanical properties of HPG-backfill. These methods included uniaxial compressive strength (UCS) testing, mass loss measurements, X-ray diffraction (XRD), thermogravimetric and differential thermogravimetric (TG-DTG), scanning electron microscopy-energy dispersive X-ray spectroscopy (SEM-EDS), and nuclear magnetic resonance (NMR). The experimental and analytical processes are shown in Fig. 5, and the specific procedures are briefly described below.

(1) **UCS test**. The 28-day strength of the backfill, critical for two-step ore mining, was examined. The initial phase of the study focused on a 28-day curing period, with plans for further long-term testing (i.e., a 90-day test) to assess the ion leaching behavior of HPG. Samples were cured at 20±2°C and 90 % relative humidity as the control group, while others were submerged in MW at various temperatures and pH levels for 28 days. UCS tests were performed using a YAW-300C automatic pressure testing machine with a load capacity of 100 kN and a loading rate of 0.1 mm/min.

(2) **Statistical analysis**. Regression fitting was used to model the relationship between UCS and the pH and temperature of MW. Grey relational analysis evaluated the influence of pH and temperature on UCS, providing a comprehensive understanding of their interaction with HPG-backfill's mechanical properties. Standard deviations and confidence intervals were calculated to validate the significance of the observed trends.

(3) **Mass loss test.** The mass of HPG-backfill was measured before and after submersion in MW to assess mass variation. Freshly demolded backfill samples were dried at 45°C for 48 h, and the initial mass (M_0) was recorded. After 28 days of curing and submersion, the specimens were dried again, and the final mass (M_1) was recorded. The mass loss rate (m_l) was then calculated as:

$$m_l = \frac{M_1 - M_0}{M_0} \tag{1}$$

Table 1
Experimental design.

Number	Mix composition (%)			MW	
	Mass concentration	Quicklime/HPG	Tailings/HPG	Temperature (°C)	pH
N1	66	4	10	-	-
N2	66	4	10	20	7
N3	66	4	10	30	7
N4	66	4	10	40	7
N5	66	4	10	20	5
N6	66	4	10	30	5
N7	66	4	10	40	5
N8	66	4	10	20	3
N9	66	4	10	30	3
N10	66	4	10	40	3

(4) **XRD**. Phase analysis was performed using a Smartlab X-ray diffractometer. The settings included a voltage of 40 kV, a current of 150 mA, a step size of 2θ=0.02°, and a scanning speed of 5 s/step, within an analysis range of 2θ (5°~55°). Both cured and submerged specimens were analyzed to detect phase transformations.

(5) **TG-DTG**. TG and DTG analyses were performed using an SDT Q600 instrument. Samples were heated from 30 to 890°C at a rate of 10 °C/min in a nitrogen atmosphere. The weight loss observed at different temperatures was used to infer the material's composition and content, providing insights into changes in hydration products of the HPG-backfill after exposure to MW.

(6) **SEM-EDS**. Microstructural analysis was conducted on surface-eroded fragments collected from specimens subjected to UCS testing. The fragments were carbon-coated to ensure adequate conductivity before examination using a JSM-6510 scanning electron microscope at an accelerating voltage of 20 kV. Magnifications were set at 500× and 3000×, with a resolution of 3 nm, to capture both broad morphological features and fine microstructural details. The SEM was equipped with EDS for elemental analysis, enabling the assessment of compositional changes alongside morphological alterations.

(7) **NMR**. Pore structure distribution was assessed using a Meso-MR23–060H-I NMR spectrometer. Specimens were tested, and T_2 spectrum curves were recorded. The resonance frequency was set to 23 MHz, and the magnet temperature was adjustable between 25°C to 35°C, with a control accuracy of ±0.05°C, to evaluate the changes in pore size distribution under different MW conditions.

3. Results and analysis

3.1. Effect of MW temperature and pH on strength degradation of HPG-backfill

3.1.1. Analysis of single parameters effects

The strength of HPG-backfill specimens after 28 days of standard curing is 2.15 MPa. However, as shown in Fig. 6, when submerged in MW, the strength consistently decreased compared to standard-cured specimens, indicating a weakening effect of MW on mechanical properties of the backfill. Furthermore, as the pH of the MW decreases and the temperature increases, the backfill' strength further declines. Specifically, the compressive strength decreases by up to 52.5 % at pH=3 and by 54.8 % at 40°C when submerged in MW, compared to specimens under standard curing conditions. These results underscore the significant influence of both MW pH and temperature on the degradation of HPG-backfill strength.

To further analyze the variation in HPG-backfill strength under different conditions, a regression fitting analysis was performed. The results revealed that, when temperature was held constant, the relationship between HPG-backfill strength and MW pH could be described by a polynomial equation (Fig. 6(a)). In addition, a linear negative correlation was observed between HPG-backfill strength and MW temperature when the pH was kept constant (Fig. 6(b)).

3.1.2. Analysis of multifactor coupling effects

Multivariate nonlinear fitting was performed on the experimental data using Design-Expert software. A regression model (Eq. (2)) was established to analyze the relationship between 28-day strength of HPG-backfill and MW pH and temperature. The model demonstrated a strong fit (R^2=0.996), indicating a polynomial relationship with pH and a linear relationship with temperature. These results are consistent with the conclusions presented in Section 3.1.1, further confirming the model' accuracy. Error analysis of the predicted strength values under different conditions, shown in Fig. 7, revealed generally small errors. Although some data points show errors exceeding 15 %, these are associated with lower strength values. The majority of the predicted values closely match the experimental results, demonstrating that the model exhibits overall high reliability.

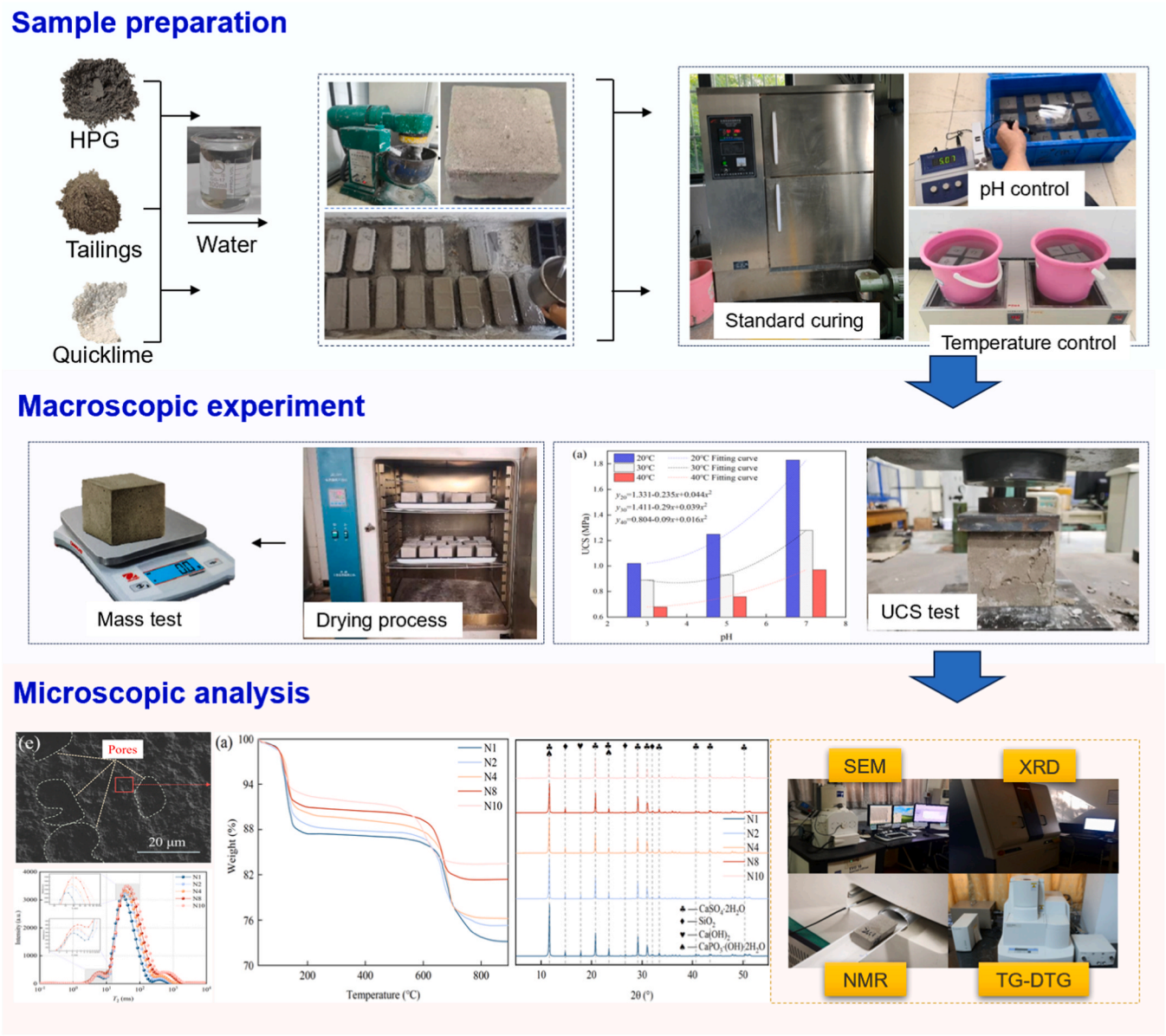

Fig. 5. Main experimental process.

$$y = 0.027x_2^2 - 0.007x_1x_2 + 0.007x_1 + 0.081x_2 + 0.88,\ R^2 = 0.996 \quad (2)$$

where y is the strength; x_1 is the MW temperature; x_2 is the MW pH.

The interactive effects of MW pH and temperature on the compressive strength of HPG-backfill were further examined through response surface, as shown in Fig. 8. While both factors significantly influence specimen strength, their interaction is not particularly significant. Specifically, at pH=7, increasing the temperature results in a noticeable decrease in sample strength, with a steeper response surface. The strength of the specimens decreased by 0.55 MPa and 0.86 MPa when the MW temperature was raised from 20°C to 30°C and 40°C, respectively. At pH=5, raising the MW temperature from 20°C to 30°C and 40°C reduced sample strength by 0.32 MPa and 0.49 MPa, respectively. At pH=3, strength decreased by 0.13 MPa and 0.34 MPa for the same temperature increases.

As the pH of the MW decreases, the increase in temperature still reduces sample strength, but the response surface becomes progressively flatter. This indicates that the interaction between temperature and pH weakens as the pH decreases. Additionally, this interaction weakened as the MW temperature increases. This may be due to the presence of Ca $(OH)_2$ in HPG-backfill (Jin et al., 2021), which can be eroded in a pH=5 acidic environments, reducing sample strength. In environments with pH=3, the internal alkaline substances may be further eroded. Although increasing the temperature raises the average kinetic energy of solvent molecules, enhancing their interaction with alkaline substances on the sample surface (Kybartiene et al., 2004). The solvent mainly consists of H^+, SO_4^{2-}, and H_2O. H^+ mainly reacts with the alkaline substances in a neutralization reaction, while SO_4^{2-} and H_2O participate in the dissolution and recrystallization of gypsum. As the temperature does not change significantly, differences in the dissolution and recrystallization processes of gypsum may not be pronounced. In acidic environments, a slight increase in temperature may not significantly deteriorate sample strength, but a general trend towards further weakening is evident.

3.1.3. Correlation analysis

The gray correlation analysis method was employed to determine the primary and secondary influences of MW temperature and pH on the compressive strength of HPG-backfill. The 28-day strength test results of the specimens served as the basis for data partitioning. The 28-day strength of HPG-backfill (X_0) was designated as the reference

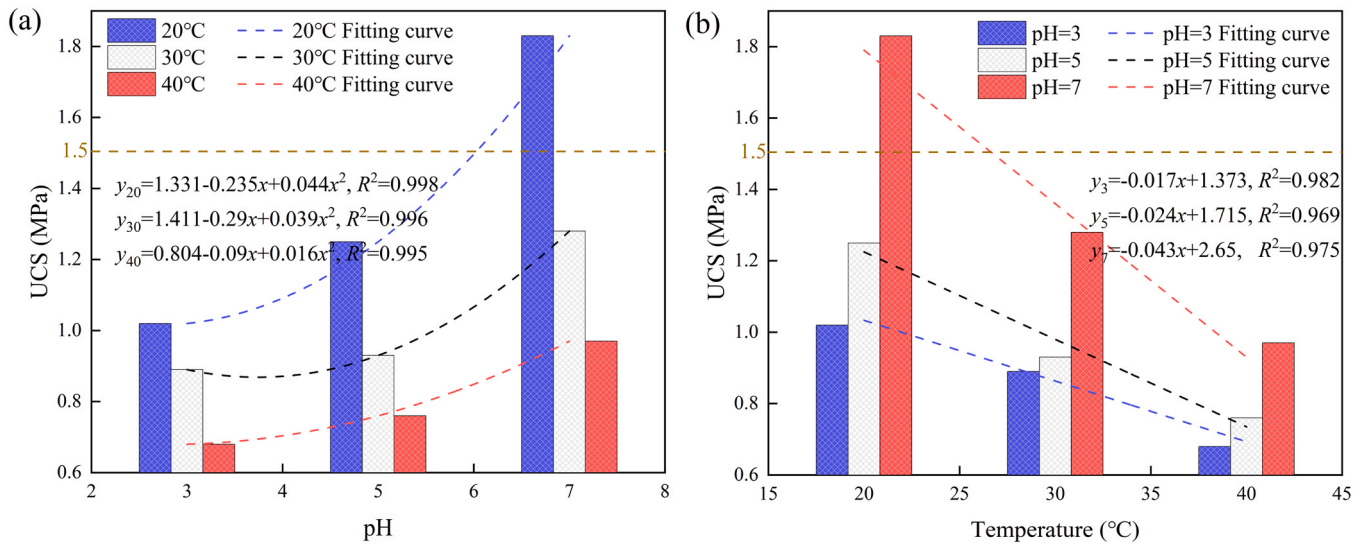

Fig. 6. Variation patterns of HPG-backfill strength: (a) Relationship between pH and strength, (b) Relationship between temperature and strength.

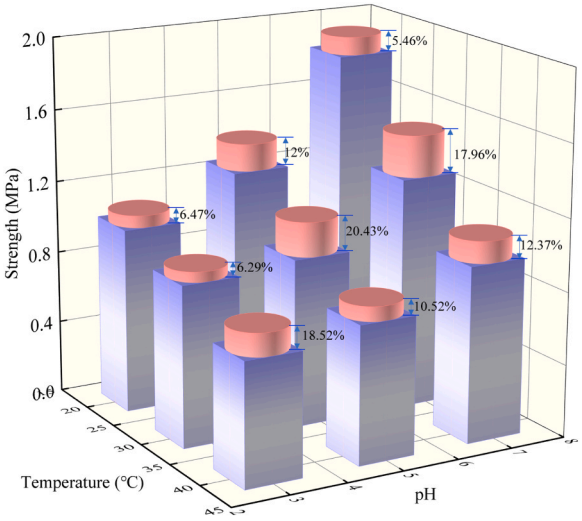

Fig. 7. Error analysis diagram.

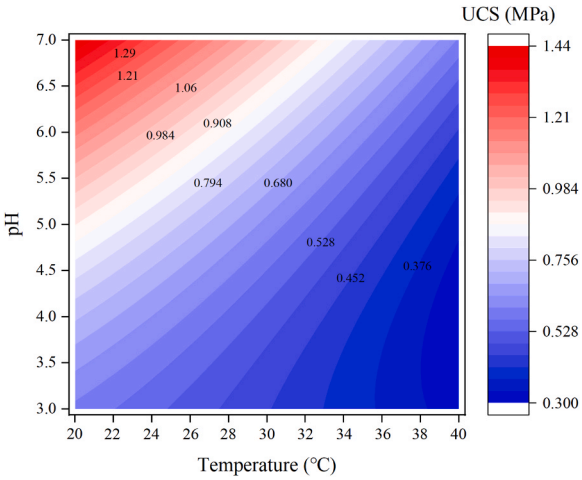

Fig. 8. Response surface plots of the effect of MW pH and temperature on the strength of HPG-backfill.

sequence. MW temperature (X_1) and pH (X_2) were designated as comparative sequences. Firstly, the data were normalized to eliminate dimensional differences. Then, the correlation coefficient $\xi_i(k)$ was calculated using Eq. (3). For detailed calculation process, can refer to the literature (Zhou et al., 2021).

$$\xi_i(k) = \frac{\min_i \min_k |X_0(k) - X_i(k)| + \rho \max_i \max_k |X_0(k) - X_i(k)|}{|X_0(k) - X_i(k)| + \rho \max_i \max_k |X_0(k) - X_i(k)|} \quad (3)$$

where ρ is the resolution coefficient, taken as 0.5; $|X_0(k) - X_i(k)|$ is the absolute difference between the reference sequence and the comparative sequence; $\min_i \min_k \Delta_i(k)$ is the minimum difference; $\max_i \max_k \Delta_i(k)$ is the maximum difference.

The gray correlation coefficients obtained in descending order are as follows: MW pH (0.7647)> MW temperature (0.6198). This indicates that among the factors of MW temperature and pH, the pH of the MW has a greater impact on the development of the 28 days' strength of HPG-backfill.

3.2. Changes in physical properties of HPG-backfill strength degradation

3.2.1. Appearance characteristics

The appearance of HPG-backfill specimens after 28 days of

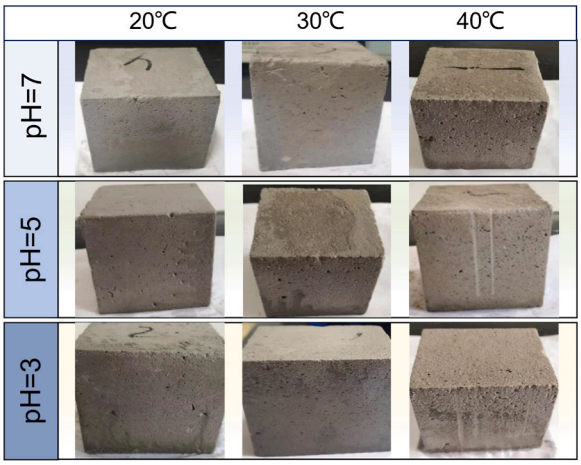

Fig. 9. The appearance of HPG-backfill after submersion in MW with different conditions for 28 days.

submersion in MW under different parameters is shown in Fig. 9. In comparison to the standard cured specimens, significant erosion was observed in submerged specimens. At 20°C, the surface exhibited more visible pores compared to standard conditions, although the overall texture remained relatively smooth (see Fig. 5). At 30°C, surface pores became more pronounced, and further pore enlargement occurred at 40°C, indicating a clear relationship between increased temperature and surface degradation.

As MW pH decreased, the severity of surface erosion intensified. At pH=3 and 40°C, extensive aggregate detachment and severe surface roughness was observed. This rougher texture is likely a result of increased dissolution of $Ca(OH)_2$ and $CaSO_4•2H_2O$, accelerating the degradation process. The pronounced surface roughness and pore formation across all temperatures at lower pH levels (pH=3) supports the conclusion that acidic MW significantly contributes to strength degradation.

3.2.2. Mass change

As shown in Fig. 10, after 28 days of standard curing, HPG-backfill exhibited a mass increase of 3.81 %. However, after 28 days of submersion in MW at pH=7 and 20°C, the mass loss was only 1.02 %, which can be attributed to the slight solubility of gypsum and the ongoing hydration reactions that convert hemihydrate gypsum into gypsum dihydrate (Chen et al., 2022; Zhou et al., 2020). The formation of $CaSO_4•2H_2O$ and residual $Ca(OH)_2$ results in minimal mass loss despite the dissolution of gypsum.

At pH=3, the mass loss rate increased to 2.29 %, showing that acidic MW accelerates mass loss due to the neutralization reaction between H^+ ions and $Ca(OH)_2$, as well as the dissolution of gypsum. When the temperature is further increased to 40°C under the same pH conditions, the mass loss reaches 6.43 %. This substantial increase is explained by the "S-shaped" solubility curve of gypsum, where solubility rises rapidly with temperature, leading to accelerated dissolution and mass loss of the HPG-backfill (Wang et al., 2020a,b).

3.3. Changes in microstructure and mineralogy of HPG-backfill strength degradation

3.3.1. Mineralogical composition analysis

The XRD results for HPG-backfill, both under standard curing and submerged in MW with different parameters for 28 days, are presented in Fig. 11. The primary hydrated products of HPG-backfill under standard curing conditions include $CaSO_4•2H_2O$, $Ca(OH)_2$, SiO_2, and insoluble phosphates ($CaPO_3(OH)·2H_2O$). The diffraction peaks of gypsum crystals are sharp at approximately 11°, 21°, and 29° (Adrien et al., 2016).

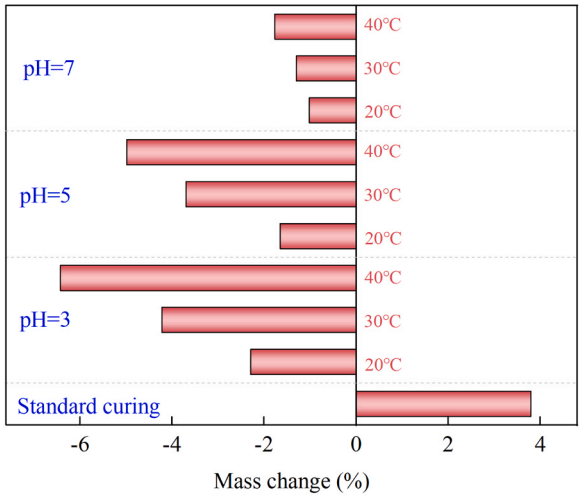

Fig. 10. Mass changes of HPG-backfill after exposure to MW under different conditions for 28 days.

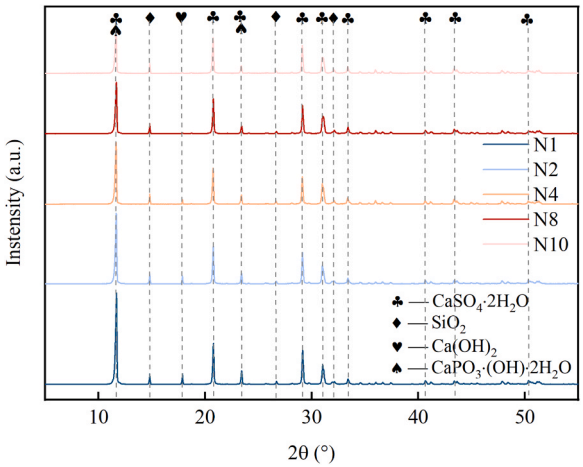

Fig. 11. XRD results of the outer surface layer of HPG-backfill after submersion in MW under different conditions.

After submersion in neutral MW (pH=7, 20℃), these peaks exhibit reduced intensity, indicating partial dissolution of gypsum. This corresponds with the mass loss described in Section 3.2.2. The decrease in peak intensity is more pronounced at pH=3 and 20°C, as the acidic MW accelerates gypsum dissolution by breaking the bonds between water molecules and calcium-sulfate ions (Duan et al., 2017). The disappearance of $Ca(OH)_2$ peaks further supports the dissolution reaction between H^+ and $Ca(OH)_2$, which exposes gypsum crystals to further degradation (Li et al., 2018a,b).

The inert nature of SiO_2 and insoluble phosphates is demonstrated by the unchanged peak intensity across all conditions. Additionally, raising the MW temperature from 20°C to 40°C led to further weakening of $CaSO_4•2\ H_2O$ peaks, reflecting temperature-driven dissolution. The higher kinetic energy at elevated temperatures increases the rate of solvent-ion interaction, facilitating the breakdown of gypsum crystals.

3.3.2. TG-DTG analysis

Fig. 12 shows the TG and DTG curves of HPG-backfill after standard curing and after 28 days of submersion in MW with different parameters. The thermal decomposition of HPG-backfill primarily occurs within the ranges of 30°C to 260°C and 430°C to 830°C, corresponding to two endothermic peaks. This indicates that the thermal decomposition process involves two main stages.

At the first stage, the mass loss mainly originates from the dihydrate gypsum in the hydrated products. The standard cured samples exhibit higher weight loss and endothermic peak values. As the temperature of the MW increases or pH decreases, these peak values decrease, suggesting that the standard cured samples contain more hydrated products than the samples submerged in MW with different parameters (Wang et al., 2020a,b). This suggests that higher temperatures or lower pH levels cause more severe erosion of the hydration products.

At the second stage, the mass loss primarily originates from the endothermic decomposition of the main mineral component in the tailings, which is calcite. The endothermic peak values between 430°C and 830°C decrease as the temperature of the MW increases or pH decreases. Although calcite is inert and typically does not react with acids, this decrease may relate to increased surface porosity and detachment of tailings caused by intensified erosion. This detachment leads to a reduction in the endothermic peak values of calcite, aligning with the observations on appearance characteristics and mass loss described in Sections 3.2.1 and 3.2.2.

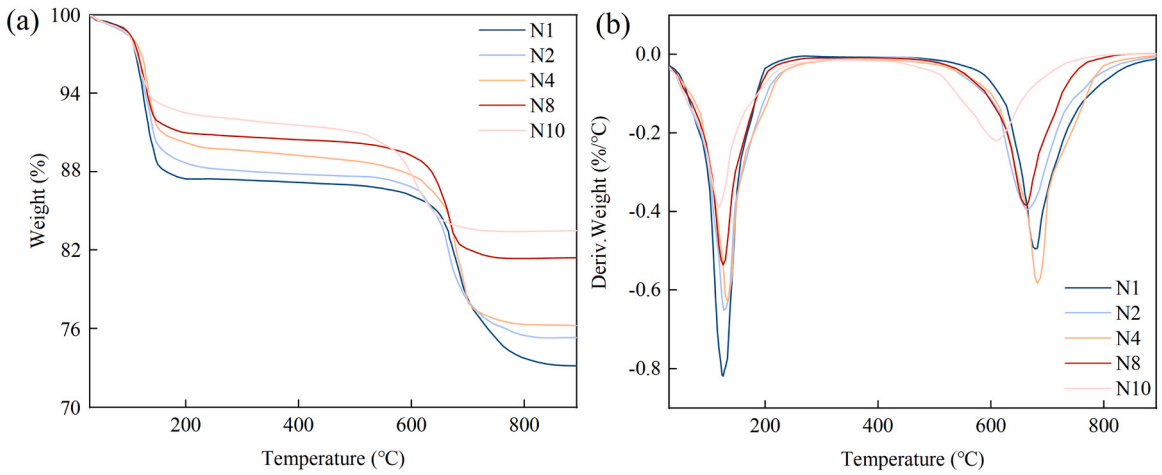

Fig. 12. TG and DTG curves of HPG-backfill under different conditions: (a) TG curve, (b) DTG curve.

3.3.3. Microstructure analysis

SEM analysis of the corroded areas on the surface layer of the specimens with standard curing and after 28 days of submersion in MW with different parameters is shown in Fig. 13. The surface of standard cured samples appears smooth and compact (Fig. 13(a)). Samples submerged in neutral MW (pH=7, 20℃) exhibit initial surface irregularities (Fig. 13(c)). As the pH decreases to 3, the number of holes due to acidic erosion increases, with these holes extending towards the inner layers of the sample (Fig. 13(e)). At higher magnifications, not-submerged samples show numerous long rod-shaped and short columnar crystals with a high degree of interlocking, indicating a dense structure (Fig. 13(b)). EDS analysis identified the main elements in the long rod-shaped crystals as Ca, S, and O, confirming them as gypsum dihydrate crystals (Maierdan et al., 2021; Min et al., 2019). After submersion in MW, these long rod-shaped crystals decrease, suggesting that the MW's dissolving effect reduces the length-to-diameter ratio of the original gypsum dihydrate crystals. Short columnar gypsum dihydrate crystals remain abundance (Fig. 13(d)). As MW acidity intensifies, fragmented crystals and fine short crystals increase, reducing the degree of interlocking and loosening the structure (Fig. 13(f)) (Geng et al., 2015; Nadelman et al., 2019).

When the MW temperature increases to 40°C, the degree of surface corrosion worsens, and the pores' size increases (Fig. 13(g)). At pH=3 and 40°C, severe surface corrosion occurs, with numerous pores extending deeply into the samples, forming invasion channels (Fig. 13 (i)). These microscopic changes indicate that higher temperatures result in more severe structural corrosion by MW. Particularly, corrosion intensifies when the temperature increase coincides with a pH decrease. At 3000x magnification, changes in crystal morphology are observed. Compared to Fig. 13(d), samples submerged in MW at 40°C show fewer short columnar and long rod-like gypsum dihydrate crystals, with an increase in irregularly shaped fragmented crystals (Fig. 13(h)). At pH=3 and 40°C, many fragmented crystals appear, with almost no short columnar and long rod-like crystals remaining (Fig. 13(j)). These results indicate that increasing MW temperature or decreasing pH alters gypsum dihydrate crystal morphology and pore structure, reducing the structural compactness of HPG-backfill and leading to a decrease in its compressive strength.

3.3.4. Pore structure analysis

The transverse relaxation time (T_2) provides insights into the microscopic pore structure of HPG-backfill (Li et al., 2018a,b). The T_2 was plotted against the inversion signal intensity to investigate the effect of different parameters of MW on the pore structure of HPG-backfill, as shown in Fig. 14. According to Eq. (4), a larger T_2 value implies a larger pore diameter (Zeng et al., 2023). The three main signal peaks in the T_2 relaxation spectrum can be categorized from left to right as representing small, medium, and large pores.

$$\frac{1}{T_2} = \alpha\left(\frac{3}{R}\right) \tag{4}$$

where α is the surface relaxation strength, with an empirical value of 5 μm/ms; R is the pore radius, cm.

Compared to non-submerged sample, the signal intensity of medium and large pores increased significantly after 28 days of MW exposure, indicating pore expansion due to erosion (Li et al., 2019). This expansion was most pronounced at higher temperatures, with the peak for medium pores intensifying at 40°C, confirming that elevated temperatures accelerate internal erosion (Liu et al., 2024). Similarly, as pH decreased, the signal intensity across all pore sizes increased, with the most severe pore structure deterioration observed at pH=3 and 40°C. These results show that both high temperatures and acidic conditions exacerbate pore expansion and generation.

Based on NMR principles, the total area under each inversion curve corresponds to the porous volume of the sample (Zhu et al., 2024). To quantify the effect of MW with different parameters on the sample's pores, the porosity change rate γ is introduced, as calculated by Eq. (5). The relationship between γ and MW parameters is shown in Table 2. The results indicate that the γ is greater than 0 for all samples submerged in MW, indicating an increase in internal pores. When the sample was submerged in neutral MW at 20°C, the internal pore volume increased by 38 %. As the MW temperature increased and the pH decreased, the internal pore volume continued to rise. For the sample submerged in MW with a pH=3 and a temperature of 40°C, the internal pore volume reached 2.93 times that of the standard cured sample.

$$\gamma = \frac{P - P_0}{P_0} \times 100\% \tag{5}$$

where P_0 is the area under the inversion curve of the standard cured sample; P is the area under the inversion curve of the sample submerged in MW with different parameters.

4. Discussions

4.1. Mechanism of the effect of MW temperature on the HPG-backfill strength degradation

The influence of MW temperature on HPG-backfill degradation needs to be contextualized with respect to MW at ambient temperature. When HPG-backfill is submerged in neutral MW (pH=7) at 20℃, the gypsum dihydrate crystals within the backfill slowly dissolve due to the

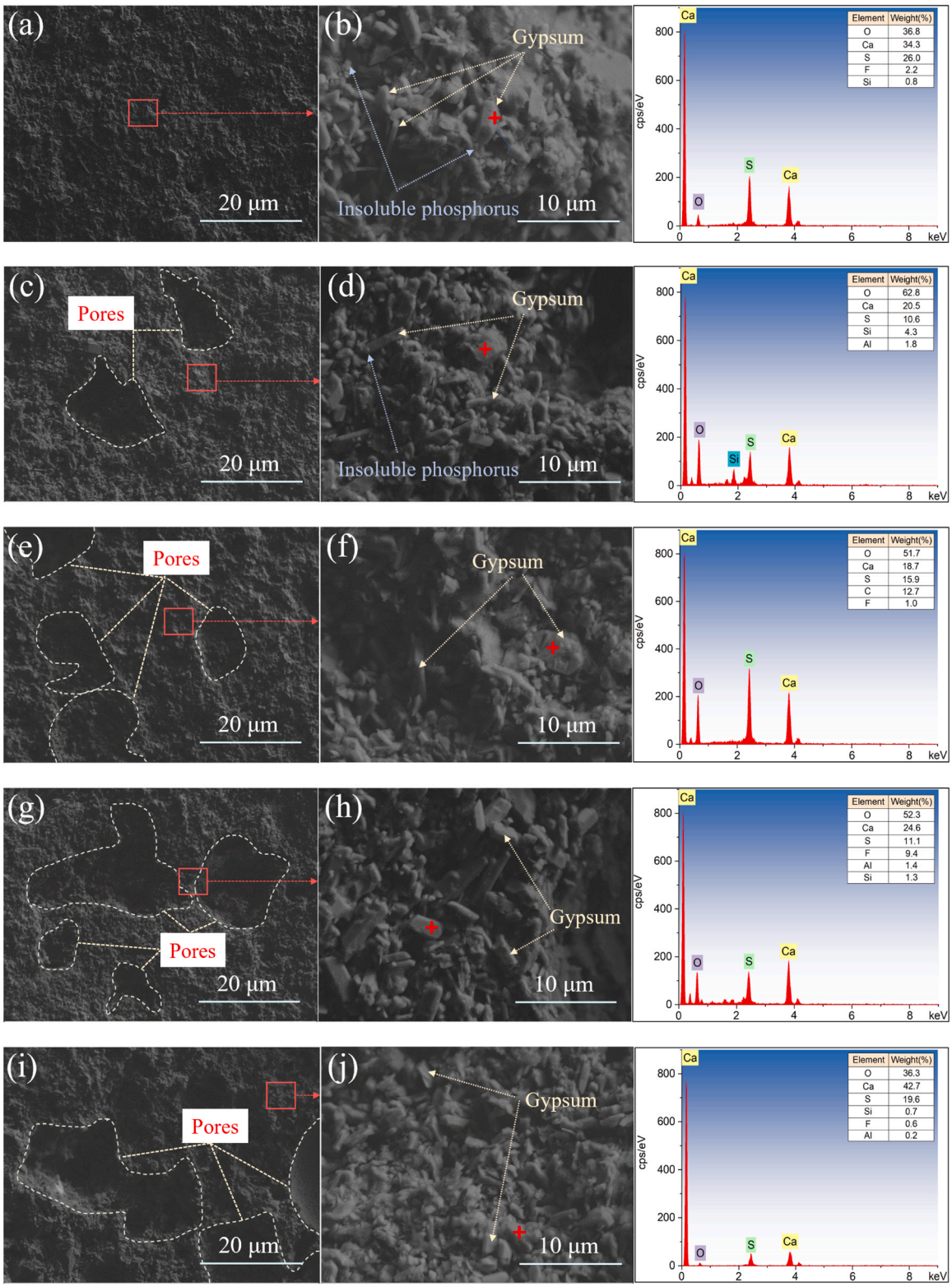

Fig. 13. SEM image showing the outermost layer of HPG-backfill after 28 days of exposure to MW: (a) N1 (× 500), (b) N1 (× 3000), (c) N2 (× 500), (d) N2 (× 3000), (e) N4 (× 500), (f) N4 (× 3000), (g) N8 (× 500), (h) N8 (× 3000), (i) N10 (× 500), (j) N10 (× 3000).

concentration gradient. In addition, the evaporation of excess water during the exothermic hydration process creates pores in the HPG-backfill, potentially providing capillary channels for MW to erode the sample's interior. As a result, MW first dissolves the surface material and then penetrates into the sample, breaking down the internal gypsum crystal structure. At the same time, a water film forms on the crystal surfaces, which can penetrate the microcracks of the gypsum. This intrusion disrupts the micro-pore bonding between crystal structures, ultimately weakening the inter-crystal bonding force (Tian et al., 2016). This inherent characteristic of poor water resistance in gypsum results in the reduced strength of HPG-backfill after submersion in MW (Singh, 2003a, 2005b).

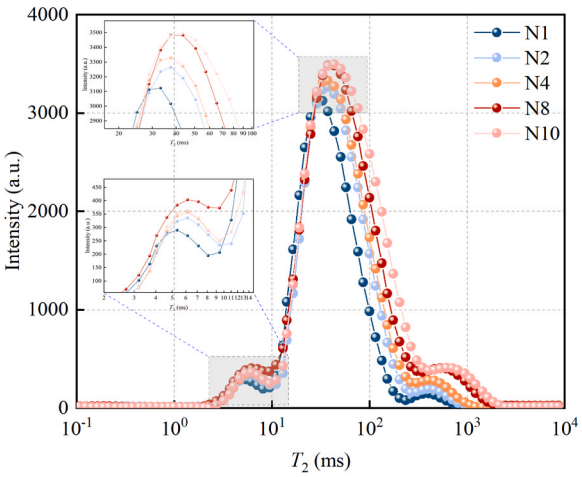

Fig. 14. NMR relaxation spectrum of HPG-backfill.

Table 2
Peak area of inversion curve of HPG-backfill.

Number	Peak area of inversion curve	γ value
N1	360428	0
N2	498200	38 %
N4	577559	60 %
N8	938096	160 %
N10	1055140	193 %

When HPG-backfill is submerged in high-temperature MW, as described in Section 3.2.2, the solubility of gypsum increases. Macroscopically, this manifests as an enhanced erosive effect of high-temperature MW on the sample, as shown in Fig. 15. This is because temperature is a macroscopic measure of the average kinetic energy of molecules (Aich et al., 2024). Consequently, the frequency of collisions between water molecules and gypsum crystals per unit time also increases, leading to a higher probability of dissolving gypsum crystals. Rising temperature intensifies the interaction between the ions on the surface of gypsum crystals and MW. Furthermore, the rapid, continuous alternation of crystallization pressure during the dissolution-recrystallization process at higher temperatures contributes to the fatigue damage of the sample. The crystal growth process itself is a thermodynamic phase transition. The crystallization process releases heat, causing the surrounding MW temperature to rise and the solubility to increase. The dissolution process of crystals absorbs heat, resulting in a decrease in the surrounding MW temperature and solubility. This alternating temperature change during the dissolution-recrystallization process leads to alternating changes in solution supersaturation. Consequently, the crystallization pressure exerted by the crystals on the pore walls alternates between increasing and decreasing (Kaufmann et al., 2004). Under high-temperature conditions, the reaction rate accelerates, leading to rapid dissolution-recrystallization of gypsum crystals. The rapid alternation of crystallization pressure induces fatigue cracks in the sample, which expand and extend inward with continued exposure.

4.2. Mechanism of the effect of MW pH on the HPG-backfill strength degradation

When the MW environment changes from neutral to acidic, the H^+ ions in the MW rapidly neutralize the alkaline substances on the sample's surface. As the submersion time extends, the alkaline substances on the surface will be completely neutralized. This will entirely expose the gypsum on the surface to the acidic MW, and accelerating the dissolution process of gypsum. This results more pores and cracks appearing on the sample surface, leading to an uneven texture. With the increasing acidity of the MW, H^+ gradually erode the alkaline substances on the outer surface of the sample, completely exposing the outer surface of the sample to the acidic MW. This process facilitates the continued corrosion of the sample's internal structure by H^+ ions, generating pore channels that extend deeper into the inner layers of the sample, as shown in Fig. 16.

The deeper reasons for these phenomena may require further analysis. According to the principle of energy conservation and Correns' equation (Correns, 1949), the solubility of a crystal increases with higher free energy and curvature. This increase in solubility results in a higher concentration of solute in the surrounding MW solution. Different crystal curvatures result in concentration gradients in the surrounding salt solutions. Fick's second law states that ions in the free solution at the crystal's end diffuse one-dimensionally from high to low concentration along the capillary pores. During the standard curing of HPG-backfill, gypsum crystals grown in the pores are subjected to the effects of diffusion, crystal free energy, and the pressure exerted by the capillary pore wall on the crystals. As a result of these interacting factors, crystals will grow towards the unconstrained direction or the free end along the pore axis. Meanwhile, adjacent crystals may gradually merge into one, growing in a columnar or rod-like manner, thereby gradually increasing in volume (see Fig. 13(b)). At this point, the pores between the crystals mainly exist in a variable cross-sectional form, typically smaller at both ends and larger in the middle (Gou et al., 2023). Under acidic conditions, gypsum crystals undergo dissolution-recrystallization, with the pores between the crystals mainly exist in a variable cross-sectional form. There is a difference in supersaturation between the borders and the core. During crystallization, salt solution first crystallizes in the larger pores of the belly, and then the crystals grow rapidly at both ends of the pores. Dissolution begins at the smaller pores of the capillary opening. Due to the presence of a large amount of SO_4^{2-} in acidic MW, gypsum crystallization is induced prematurely. This results in the changes in the morphology and pore structure of gypsum crystals, leading to the appearance of numerous lamellar or fragmented gypsum crystals (see Fig. 13(h) and (j)) (Yang et al., 2016). In conclusion, the strength deterioration of samples in acidic MW is mainly due to the erosion of alkaline substances and changes in crystal morphology and

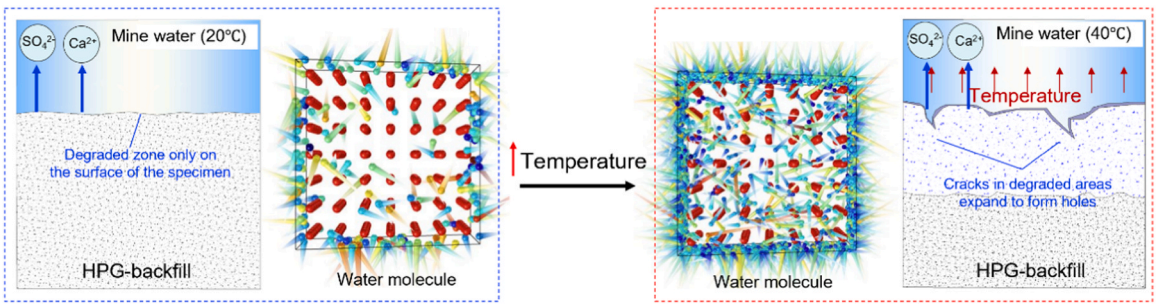

Fig. 15. Schematic diagram of the erosion of HPG-backfill under different MW temperatures.

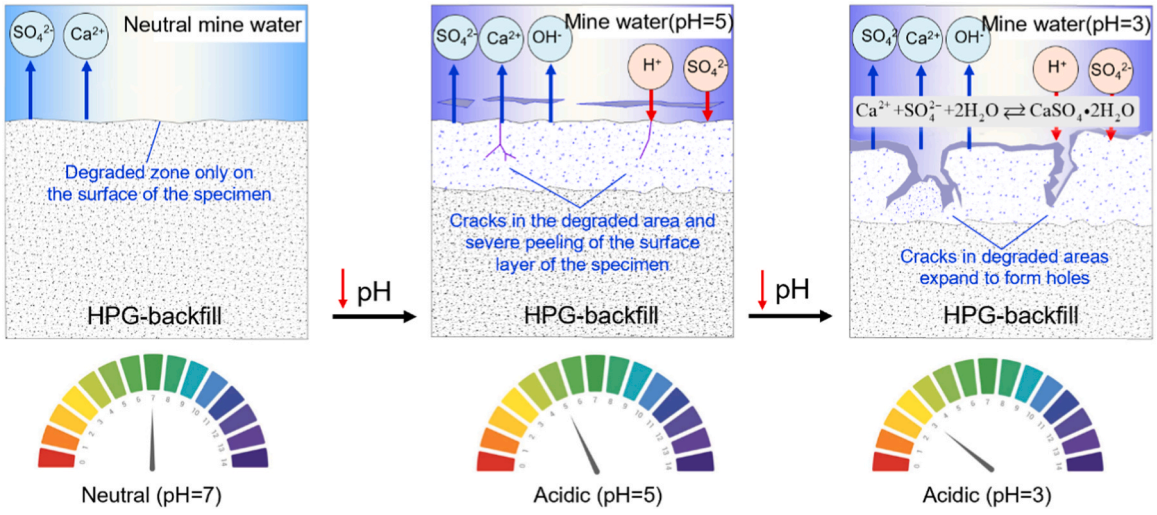

Fig. 16. Schematic diagram of HPG-backfill erosion by MW.

pore structure from the dissolution-recrystallization process, reducing HPG-backfill's structural density.

4.3. Mechanism of interaction effects on the HPG-backfill strength degradation

From the experimental results in Section 3.2.2, it can be observed that the combined effect of temperature and pH of MW results in a synergistic degradation of HPG-backfill. This accelerates the deterioration process of the backfill strength. This process involves interactions between the thermal, hydraulic, mechanical, and chemical fields, as shown in Fig. 17. Firstly, the increase in MW temperature accelerates the chemical reaction rate of acidic MW eroding HPG-backfill, leading to faster dissolution of gypsum and accelerated erosion of internal alkaline substances. In addition, as described in Section 4.1, temperature variations cause alternating changes in supersaturation during gypsum dissolution and recrystallization processes, thereby generating crystallization pressure. The alternating changes in crystallization pressure are prone to induce fatigue cracks in the samples. This provides pathways for acidic MW to further infiltrate into the sample, accelerating internal erosion. Over time, these physical and chemical processes act together to gradually erode the structure of HPG-backfill, leading to a gradual reduction in strength and durability.

To mitigate the detrimental effects of acidic MW at elevated temperatures on HPG-backfill, mining operators can adopt several strategies to enhance the durability and long-term performance of backfill materials. One effective approach is incorporating additives or modifiers into the HPG-backfill formulation, aimed at increasing resistance to acidic conditions and reducing solubility. For instance, the addition of pozzolanic materials (e.g., fly ash, silica fume) or cementitious agents (e.g., blast furnace slag) can significantly improve the chemical stability and mechanical strength of the backfill (Wang et al., 2022a; Wu et al., 2020; Zhang et al., 2023). These materials promote the formation of secondary hydration products that fill pores and enhance the overall matrix, making the backfill less susceptible to acid-induced degradation and thermal stress.

Another practical method is pH optimization of the MW through treatment technologies such as neutralization. This can be achieved by adding alkaline substances (e.g., lime, limestone) to the MW which raises its pH and mitigates its corrosive potential (Mohan and Dutta,

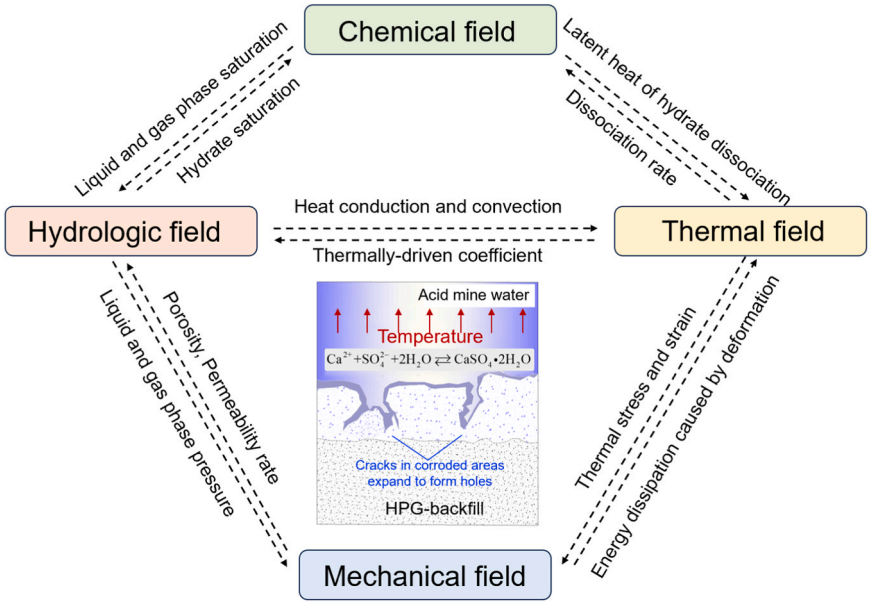

Fig. 17. Interactions between thermal, hydraulic, mechanical and chemical fields.

2020; Suthar and Aggarwal, 2018). Neutralizing the MW can reduce the rate of dissolution and erosion of the backfill, thereby extending its service life in mining operations. Such treatment processes could be implemented on-site, ensuring that MW interacting with the backfill maintains a less aggressive pH range.

In addition to these methods, improvements in backfill material composition offer a promising avenue for mitigating the combined effects of acidity and high temperatures. The development of advanced backfill formulations incorporating fibers (e.g., polypropylene, glass, or carbon fibers) can enhance the mechanical strength and crack resistance of the material (Ari et al., 2023; Rudrappa and Srinivasachar, 2020). These fibers act as reinforcement, reducing crack propagation and improving tensile strength, especially under thermal and acidic stress. These approaches, combined with monitoring systems for pH and temperature, will allow operators to implement real-time adjustments, optimizing backfill performance in harsh mining conditions.

5. Conclusions and future work

The influence of MW at different temperatures and pH on the mechanical strength of HPG-backfill was systematically evaluated, revealing significant weakening effects. UCS tests conducted on HPG-backfill submerged in MW for 28 days indicated a polynomial correlated between strength and MW pH, and a linear correlation with temperature. In addition, response surface methodology identified an interaction between MW temperature and pH that negatively impacts the backfill's strength.

Microscopic analyses using XRD, TG-DTG, SEM-EDS, and NMR revealed the mechanisms behind these observations. Strength degradation at elevated temperatures may be associated with crystallization pressure generated during the gypsum dissolution and recrystallization process, which induces fatigue cracks in the samples. The presence of high concentrations of SO_4^{2-} under acidic conditions promotes premature gypsum crystallization, altering crystal morphology and pore structure. Moreover, the submersion of HPG-backfill in acidic MW at high temperatures may involve interactions among thermal, hydraulic, mechanical, and chemical fields.

Continuous monitoring and regulation of MW pH are crucial to maintain conditions within a less corrosive range. Implementing pH control systems, including the application of alkaline additives, can effectively neutralize acidic environments. Optimizing ventilation and thermal insulation in mining operations also helps manage temperature fluctuations, thereby reducing the impact of elevated temperatures on backfill integrity. These measures collectively aim to mitigate degradation mechanisms and promote the durability of backfill materials under variable mining conditions.

Despite the valuable insights gained from this study, certain limitations should be acknowledged. The research primarily focused on specific pH levels and temperature ranges, which may not fully represent the range of conditions encountered in diverse mining environments. Additionally, the interactions among various MW constituents and their cumulative effects on HPG-backfill were not fully examined. Future research should explore these interactions and investigate the impact of other MW constituents, such as dissolved ions and organic matter, on backfill degradation. Furthermore, developing advanced backfill materials with improved resistance to acidic and high-temperature environments will be critical for ensuring the long-term stability and performance of backfill in mining operations.

CRediT authorship contribution statement

Aixiang Wu: Resources, Funding acquisition. **Zhikai Wang:** Writing – original draft, Methodology, Investigation, Funding acquisition, Formal analysis, Data curation, Conceptualization. **Yiming Wang:** Writing – review & editing, Validation, Supervision, Funding acquisition, Formal analysis, Conceptualization. **Giovanna Antonella Dino:** Writing – review & editing, Supervision, Methodology. **Lianfu Zhang:** Writing – review & editing, Supervision, Methodology. **zhuen Ruan:** Writing – review & editing, Supervision, Formal analysis. **Minzhe Zhang:** Software, Data curation. **Jianqiu Li:** Resources, Methodology.

Declaration of Competing Interest

The authors declare that they have no known competing financial interests or personal relationships that could have appeared to influence the work reported in this paper.

Acknowledgments

This work was financially supported by the National Natural Science Foundation of China (Grant No. 52374111), the Natural Science Research Project of Anhui Educational Committee (Grant No. 2023AH051212), Anhui Provincial Natural Science Foundation (Grant No. 2408085QE174), and the Key Program of National Natural Science Foundation of China (Grant No. 52130404). We acknowledge the support from the China Scholarship Council (Grant No. 202306460058).

References

Adrien, J., Meille, S., Tadier, S., Maire, E., Sasaki, L., 2016. In-situ X-ray tomographic monitoring of gypsum plaster setting. Cem. Concr. Res. 82, 107–116. https://doi.org/10.1016/j.cemconres.2015.12.011.

Aich, W., Basem, A., Sultan, A., Ghabra, A., Eladeb, A., Kolsi, L., Salahshour, S., Baghaei, S., 2024. Investigation of the effect of model structure type on the thermal performance of phase change materials through molecular dynamics simulation. Case. Stud. Therm. Eng. 56, 104226. https://doi.org/10.1016/j.csite.2024.104226.

Aiken, T., Kwasny, J., Sha, W., Soutsos, M., 2018. Effect of slag content and activator dosage on the resistance of fly ash geopolymer binders to sulfuric acid attack. Cem. Concr. Res. 111, 23–40. https://doi.org/10.1016/j.cemconres.2018.06.011.

Ari, A., Bayram, A., Karahan, M., Karagöz, S., 2023. Comparison of the mechanical properties of chopped glass, carbon, and aramid fiber reinforced polypropylene. Polym. Polym. Compos 30, 1–13. https://doi.org/10.1177/0967391122109857.

Arjomandi, A., Mousavi, R., Tayebi, M., Nematzadeh, M., Gholampour, A., Aminian, A., Gencel, O., 2023. The effect of sulfuric acid attack on mechanical properties of steel fiber-reinforced concrete containing waste nylon aggregates: Experiments and RSM-based optimization. J. Build. Eng. 64, 105500. https://doi.org/10.1016/j.jobe.2022.105500.

Bharat, A., Singh, A., Mahato, M., 2024. Heavy metal geochemistry and toxicity assessment of water environment from Ib valley coalfield, India: Implications to contaminant source apportionment and human health risks. Chemosphere 352, 141452. https://doi.org/10.1016/j.chemosphere.2024.141452.

Bouargane, B., Oubelhas, I., Moreno, S.P., Biyoune, M.G., Bakiz, B., Bolivar, J.P., Atbir, A., 2023. Process of preparing chloride-free KNS compound fertilizers from phosphogypsum waste using a quaternary phase diagram. Process Saf. Environ. Prot. 177, 995–1005. https://doi.org/10.1016/j.psep.2023.07.037.

Chen, Q., Zhang, Q., Fourie, A., Xin, C., 2017. Utilization of phosphogypsum and phosphate tailings for cemented paste backfill. J. Environ. Manag. 201, 19–27. https://doi.org/10.1016/j.jenvman.2017.06.027.

Chen, X., Wang, Q., Wu, Q., Xie, S., Tang, X., Yang, G., Luo, L., Yuan, H., 2022. Hydration reaction and microstructural characteristics of hemihydrate phosphogypsum with variable pH. Constr. Build. Mater. 316, 125891. https://doi.org/10.1016/j.conbuildmat.2021.125891.

Correns, C., 1949. Growth and dissolution of crystals under linear pressure. Discuss. Faraday Soc. 5, 267. https://doi.org/10.1039/df9490500267.

Davila, J., Sarmiento, A., Fortes, J., Santisteban, M., Leiva, M., Cordoba, F., Cabello, J., Grande, J., 2021. Determination of the extreme reduction of concrete strength due to acid mine water by laboratory tests on specimens located in a real environment. Constr. Build. Mater. 269, 121817. https://doi.org/10.1016/j.conbuildmat.2020.121817.

Degirmenci, N., Okucu, A., Turabi, A., 2007. Application of phosphogypsum in soil stabilization. Build. Environ. 42, 3393–3398. https://doi.org/10.1016/j.buildenv.2006.08.010.

Deng, H., Xiao, Y., 2024. Experimentation of Heat-Insulating Materials for Surrounding Rocks in Deep Mines and Simulation Study of Temperature Reduction. Minerals 14, 938. https://doi.org/10.3390/min14090938.

Duan, Z., Li, J., Li, T., Zheng, S., Han, W., Geng, Q., Guo, H., 2017. Influence of crystal modifier on the preparation of α-hemihydrate gypsum from phosphogypsum. Constr. Build. Mater. 133, 323–329. https://doi.org/10.1016/j.conbuildmat.2016.12.060.

El-Didamony, H., Gado, H.S., Awwad, N.S., Fawzy, M.M., Attallah, M.F., 2013. Treatment of phosphogypsum waste produced from phosphate ore processing. J. Hazard. Mater. 244, 596–602. https://doi.org/10.1016/j.jhazmat.2012.10.053.

Fall, M., Pokharel, M., 2010. Coupled effects of sulphate and temperature on the strength development of cemented tailings backfills: Portland cement-paste backfill. Cem. Concr. Comp. 32, 819–828. https://doi.org/10.1016/j.cemconcomp.2010.08.002.

Geng, J., Easterbrook, D., Li, L., 2015. The stability of bound chloride in cement paste with sulfate attack. Cem. Concr. Res. 68, 211–222. https://doi.org/10.1016/j.cemconres.2014.11.010.
Gou, M., Zhao, J., Zhou, L., Hou, W., Zhao, M., 2023. Effect of succinic acid on the preparation of α-HH and its hydration properties. J. Cryst. Growth 617, 127286. https://doi.org/10.1016/j.jcrysgro.2023.127286.
He, M., Guo, P., 2013. Deep rock mass thermodynamic effect and temperature control measures. Chin J Rock Mech Eng. 32, 2377-2393 (in Chinese). https://doi.org/10.3969/j.issn.1000-6915.2013.12.001.
Holanda, F.D.C., Schmidt, H., Quarcioni, V.A., 2017. Influence of phosphorus from phosphogypsum on the initial hydration of portland cement in the presence of superplasticizers. Cem. Concr. Comp. 83, 384–393. https://doi.org/10.1016/j.cemconcomp.2017.07.029.
Jia, R., Wang, Q., Luo, T., 2021. Reuse of phosphogypsum as hemihydrate gypsum: The negative effect and content control of H_3PO_4. Resour. Conserv. Recy. 174, 105830. https://doi.org/10.1016/j.resconrec.2021.105830.
Jiang, G., Wu, A., Wang, Y., Lan, W., 2018a. Low cost and high efficiency utilization of hemihydrate phosphogypsum: Used as binder to prepare filling material. Constr. Build. Mater. 167, 263–270. https://doi.org/10.1016/j.conbuildmat.2018.02.022.
Jiang, G., Wu, A., Wang, Y., Wang, Y., Li, J., 2022b. Determination of utilization strategies for hemihydrate phosphogypsum in cemented paste backfill: Used as cementitious material or aggregate. J. Environ. Manag. 308, 114687. https://doi.org/10.1016/j.jenvman.2022.114687.
Jiang, M., Cao, S., Yilmaz, E., 2024. Exploring microstructure and mechanical features of coupled cementitious tail-sand concrete by partial replacement of tungsten tailings. Process Saf. Environ. Prot. 190 (B), 863–875. https://doi.org/10.1016/j.psep.2024.08.100.
Jin, Z., Ma, B., Su, Y., Qi, H., Lu, W., Zhang, T., 2021. Preparation of eco-friendly lightweight gypsum: Use of beta-hemihydrate phosphogypsum and expanded polystyrene particles. Constr. Build. Mater. 297, 123837. https://doi.org/10.1016/j.conbuildmat.2021.123837.
Kacimi, L., Simon-Masseron, A., Ghomari, A., Derriche, Z., 2006. Reduction of clinkerization temperature by using phosphogypsum. J. Hazard. Mater. 137, 129–137. https://doi.org/10.1016/j.jhazmat.2005.12.053.
Kasap, T., Yilmaz, E., Sari, M., Karasu, S., 2023. Predicting long-term impact of cementitious mine fill considering sand as a copper-tailings substitution. Powder Technol. 428, 118887. https://doi.org/10.1016/j.powtec.2023.118887.
Kaufmann, J., 2004. Experimental identification of ice formation in small concrete pores. Cem. Concr. Res. 34, 1421–1427. https://doi.org/10.1016/j.cemconres.2004.01.022.
Khanal, M., Qu, Q., Zhu, Y., Xie, J., Zhu, W., Hou, T., Song, S., 2022. Characterization of Overburden Deformation and Subsidence Behavior in a Kilometer Deep Longwall Mine. Minerals 12, 543. https://doi.org/10.3390/min12050543.
Li, J., Liu, H., Ai, K., Zhu, L., 2018. An NMR-Based Experimental Study on the Pore Structure of the Hydration Process of Mine Filling Slurry. Adv. Civ. Eng. 12, 4720356. https://doi.org/10.1155/2018/4720356.
Li, W., Sun, Y., Huang, Y., Shimaoka, T., Wang, H., Wang, Y., Ma, L., Zhang, D., 2019. Evaluation of chemical speciation and environmental risk levels of heavy metals during varied acid corrosion conditions for raw and solidified/stabilized MSWI fly ash. Waste Manag. 87, 407–416. https://doi.org/10.1016/j.wasman.2019.02.033.
Li, X., Du, J., Gao, L., He, S., Gan, L., Sun, C., Shi, Y., 2017. Immobilization of phosphogypsum for cemented paste backfill and its environmental effect. J. Clean. Prod. 156, 137–146. https://doi.org/10.1016/j.jclepro.2017.04.046.
Li, X., Zhang, Q., Ke, B., Wang, X., Li, L., Li, X., Mao, S., 2018. Insight into the effect of maleic acid on the preparation of α-hemihydrate gypsum from phosphogypsum in Na_2SO_4 solution. J. Cryst. Growth 493, 34–40. https://doi.org/10.1016/j.jcrysgro.2018.04.025.
Liu, S., Wang, Y., Wu, A., Liu, P., Chang, Y., Ruan, Z., 2024. Performance evolution of alkali-activated phosphorus slag paste filling material: Effect of hemihydrate phosphogypsum content. Process Saf. Environ. Prot. 187, 736–748. https://doi.org/10.1016/j.conbuildmat.2024.136036.
Maierdan, Y., Cui, Q., Chen, B., Haque, M., Ayizekeranmu, Y., 2021. Effect of varying water content and extreme weather conditions on the mechanical performance of sludge bricks solidified/stabilized by hemihydrate phosphogypsum, slag, and cement. Constr. Build. Mater. 310, 125286. https://doi.org/10.1016/j.conbuildmat.2021.125286.
Meskini, S., Samdi, A., Ejjaouani, H., Remmal, T., 2021. Valorization of phosphogypsum as a road material: Stabilizing effect of fly ash and lime additives on strength and durability. J. Clean. Prod. 323, 129161. https://doi.org/10.1016/j.jclepro.2021.129161.
Min, C., Li, X., He, S., Zhou, S., Zhou, Y., Yang, S., Shi, Y., 2019. Effect of mixing time on the properties of phosphogypsum-based cemented backfill. Constr. Build. Mater. 210, 564–573. https://doi.org/10.1016/j.conbuildmat.2019.03.187.
Mohan, R., Dutta, R., 2020. A study of suitability of limestone for fluoride removal by phosphoric acid-crushed limestone treatment. J. Environ. Chem. Eng. 8, 104410. https://doi.org/10.1016/j.jece.2020.104410.
Nadelman, E., Kurtis, K., 2019. Durability of Portland-limestone cement-based materials to physical salt attack. Cem. Concr. Res. 125, 105859. https://doi.org/10.1016/j.cemconres.2019.105859.
Naik, N., Jupe, A., Stocks, R., Wilkinson, A., Lee, P., Kurtis, K., 2006. Sulfate attack monitored by microCT and EDXRD: Influence of cement type, water-to-cement ratio, and aggregate. Cem. Concr. Res. 36, 144–159. https://doi.org/10.1016/j.cemconres.2005.06.004.
Qu, F., Li, W., Wang, K., Zhang, S., Sheng, D., 2021. Performance deterioration of fly ash/slag-based geopolymer composites subjected to coupled cyclic preloading and sulfuric acid attack. J. Clean. Prod. 321, 128942. https://doi.org/10.1016/j.jclepro.2021.128942.
Ren, J., Zhang, L., Walkley, B., Black, J., Nicolas, R., 2022. Degradation resistance of different cementitious materials to phosphoric acid attack at early stage. Cem. Concr. Res. 151, 106606. https://doi.org/10.1016/j.cemconres.2021.106606.
Rudrappa, S., Srinivasachar, V., 2020. Significance of the type of reinforcement on the physicomechanical behavior of short glass fiber and short carbon fiber-reinforced polypropylene composites. Eng. Rep. 2, e12098. https://doi.org/10.1002/eng2.12098.
Sari, M., Yilmaz, E., Kasap, T., Karasu, S., 2023. Exploring the link between ultrasonic and strength behavior of cementitious mine backfill by considering pore structure. Constr. Build. Mater. 370, 130588. https://doi.org/10.1016/j.conbuildmat.2023.130588.
Shariati, M., Kamyab, H., Habibi, M., Ahmadi, S., Naghipour, M., Gorjinezhad, F., Mohammadirad, S., Aminian, A., 2023. Sulfuric acid resistance of concrete containing coal waste as a partial substitute for fine and coarse aggregates. Fuel 348, 128311. https://doi.org/10.1016/j.fuel.2023.128311.
Shi, Y., Cheng, L., Tao, M., Tong, S., Yao, X., Liu, Y., 2021. Using modified quartz sand for phosphate pollution control in cemented phosphogypsum (PG) backfill. J. Clean. Prod. 283, 124652. https://doi.org/10.1016/j.jclepro.2020.124652.
Singh, M., 2003a. Effect of phosphatic and fluoride impurities of phosphogypsum on the properties of selenite plaster. Cem. Concr. Res. 33, 1363–1369. https://doi.org/10.1016/S0008-8846(03)00068-1.
Singh, M., 2005b. Role of phosphogypsum impurities on strength and microstructure of selenite plaster. Constr. Build. Mater. 19, 480–486. https://doi.org/10.1016/j.conbuildmat.2004.07.010.
Suthar, M., Aggarwal, P., 2018. Bearing ratio and leachate analysis of pond ash stabilized with lime and lime sludge. J. Rock. Mech. Geotech. 10, 769–777. https://doi.org/10.1016/j.jrmge.2017.12.008.
Tian, T., Yan, Y., Hu, Z., Xu, Y., Chen, Y., Shi, J., 2016. Utilization of original phosphogypsum for the preparation of foam concrete. Constr. Build. Mater. 115, 143–152. https://doi.org/10.1016/j.conbuildmat.2016.04.028.
Tran, V., Nguyen, H., Dao, V., Hilloulin, B., Nguyen, L., Nguyen, Q., Le, T., Ly, H., 2021. Effect of temperature on the chloride binding capacity of cementitious materials. Mag. Concr. Res 73, 771–784. https://doi.org/10.1680/jmacr.19.00484.
Visrudi, H., Sharifi, Y., 2023. Resistance of Mortars Containing Waste Glass Powder as Cementitious Materials Against Sulfuric Acid. Arab J. Sci. Eng. 49, 5431–5446. https://doi.org/10.1007/s13369-023-08379-3.
Wang, C., Wang, Z., Huang, D., Huang, Q., Chen, Y., Zhang, H., Shui, Z., 2023. Recovery and recycling core of phosphogypsum: characteristic hazardous elements risk assessment and analysis. Process Saf. Environ. Prot. 170, 738–756. https://doi.org/10.1016/j.psep.2022.12.062.
Wang, D., Zhang, Q., Chen, Q., Qi, C., Feng, Y., Xiao, C., 2020. Temperature variation characteristics in flocculation settlement of tailings and its mechanism. Int. J. Min. Met. Mater. 27, 1438–1448. https://doi.org/10.1007/s12613-020-2022-3.
Wang, L., Cheng, L., Yin, S., Yan, Z., Zhang, X., 2023. Multiphase slurry flow regimes and its pipeline transportation of underground backfill in metal mine: Mini review. Constr. Build. Mater. 402, 133014. https://doi.org/10.1016/j.conbuildmat.2023.133014.
Wang, Q., Cui, Y., Xue, J., 2020. Study on the improvement of the waterproof and mechanical properties of hemihydrate phosphogypsum-based foam insulation materials. Constr. Build. Mater. 230, 117014. https://doi.org/10.1016/j.conbuildmat.2019.117014.
Wang, Z., Wang, Y., Wu, L., Wu, A., Ruan, Z., Zhang, M., Zhao, R., 2022a. Effective reuse of red mud as supplementary material in cemented paste backfill: durability and environmental impact. Constr. Build. Mater. 328, 127002. https://doi.org/10.1016/j.conbuildmat.2022.127002.
Wang, Z., Wang, Y., Zhang, M., Wu, A., Ruan, Z., Yu, G., 2023b. Effect of curing pressure on the stability of bottom cemented paste backfill under different types of barricade. Case Stud. Constr. Mater. 18, e01732. https://doi.org/10.1016/j.cscm.2022.e01732.
Wang, Z., Wang, Y., Liu, Q., Dino, A.G., Ruan, Z., Wu, A., 2024c. Impact of weak interlayer characteristics on the mechanical behavior and failure modes of cemented tailings backfill: A study on thickness, strength, and dip angle. Eng. Fail. Anal. 165, 108795. https://doi.org/10.1016/j.engfailanal.2024.108795.
Wu, L., Huang, G., Liu, W., 2020. Performance evaluation of nano-silica and silica fume on enhancing acid resistance of cement-based composites for underground structures. J. Cent. South Univ. 27, 3821–3838. https://doi.org/10.1007/s11771-020-4473-0.
Yang, L., Cao, J., Li, C., 2016. Enhancing the hydration reactivity of hemi-hydrate phosphogypsum through a morphology-controlled preparation technology. Chin. J. Chem. Eng. 24, 1298–1305. https://doi.org/10.1016/j.cjche.2016.04.006.
Yu, Y., Zhang, Y., Khennane, A., 2015. Numerical modelling of degradation of cement-based materials under leaching and external sulfate attack. Comput. Struct. 158, 1–14. https://doi.org/10.1016/j.compstruc.2015.05.030.
Zeng, Z., Ma, H., Yang, C., Zhao, K., Wang, X., Zheng, Z., 2023. Characterizing imbibition and void structure evolution in damaged rock salt under humidity cycling by low-field NMR. Eng. Geol. 328, 107371. https://doi.org/10.1016/j.enggeo.2023.107371.
Zhang, Q., Zhang, B., Chen, Q., Wang, D., Gao, X., 2021. Effects of temperatures and pH values on rheological properties of cemented paste backfill. J. Cent. South Univ. 28, 1707–1723. https://doi.org/10.1007/s11771-021-4728-4.
Zhang, S., Zhao, Y., Ding, H., Qiu, J., Guo, Z., 2021. Recycling flue gas desulfurisation gypsum and phosphogypsum for cemented paste backfill and its acid resistance. Constr. Build. Mater. 275, 122170. https://doi.org/10.1016/j.conbuildmat.2020.122170.

Zhang, Y., Yang, D., Wang, Q., 2023. Performance study of alkali-activated phosphate slag-granulated blast furnace slag composites: effect of the granulated blast furnace slag content. Arch. Civ. Mech. Eng. 23, 181. https://doi.org/10.1007/s43452-023-00724-5.

Zhang, Y., Xiao, Y., Yang, H., Wang, S., Wang, L., Qi, Z., Han, J., Hao, Q., Hu, W., Wang, J., 2024. Hydrogeochemical and isotopic insights into the genesis and mixing behaviors of geothermal water in a faults-controlled geothermal field on Tibetan Plateau. J. Clean. Prod. 442, 140980. https://doi.org/10.1016/j.jclepro.2024.140980.

Zhao, D., Zhang, B., Shen, W., Wu, M., Guan, Y., Wu, J., Zhang, Z., Zhu, J., 2021. High industrial solid waste road base course binder: Performance regulation, hydration characteristics and practical application. J. Clean. Prod. 313, 127879. https://doi.org/10.1016/j.jclepro.2021.127879.

Zhao, Y., Taheri, A., Karakus, M., Chen, Z., Deng, A., 2020. Effects of water content, water type and temperature on the rheological behaviour of slag-cement and fly ash-cement paste backfill. Int. J. Min. Sci. Technol. 30, 271–278. https://doi.org/10.1016/j.ijmst.2020.03.003.

Zhou, N., Dong, C., Zhang, J., Meng, G., Cheng, Q., 2021. Influences of mine water on the properties of construction and demolition waste-based cemented paste backfill. Constr. Build. Mater. 313, 125492. https://doi.org/10.1016/j.conbuildmat.2021.125492.

Zhou, S., Li, X., Zhou, Y., Min, C., Shi, Y., 2020. Effect of phosphorus on the properties of phosphogypsum-based cemented backfill. J. Hazard. Mater. 399, 122993. https://doi.org/10.1016/j.jhazmat.2020.122993.